

Approximate evaluations and simplified analyses of shear-mode piezoelectric modal effective electromechanical coupling

Ayech Benjeddou*

Institut Supérieur de Mécanique de Paris, 3 rue Fernand Hainaut, 93400 Saint Ouen, France

(Received January 15, 2015, Revised January 20, 2015, Accepted January 22, 2015)

Abstract. Theoretical and numerical assessments of *approximate* evaluations and *simplified* analyses of piezoelectric structures *transverse shear* modal effective electromechanical coupling coefficient (EMCC) are presented. Therefore, the latter is first introduced theoretically and its approximate evaluations are reviewed; then, *three-dimensional* (3D) and simplified *two-dimensional* (2D) plane-strain (PStrain) and plane-stress (PStress) piezoelectric constitutive behaviors of *electroded* shear *piezoceramic* patches are derived and corresponding expected *short-circuit* (SC) and *open-circuit* (OC) frequencies and resulting EMCC are discussed; next, using a piezoceramic shear sandwich beam cantilever typical benchmark, a 3D finite element (FE) assessment of different evaluation techniques of the shear modal effective EMCC is conducted, including the *equipotential* (EP) constraints effect; finally, 2D PStrain and PStress FE modal analyses under SC and OC electric conditions, are conducted and corresponding results (SC/OC frequencies and resulting effective EMCC) are compared to 3D ones. It is found that: (i) physical EP constraints reduce drastically the shear modal effective EMCC; (ii) PStress and PStrain results depend strongly on the *filling foam* stiffness, rendering inadequate the use of popular equivalent single layer models for the transverse shear-mode sandwich configuration; (iii) in contrary to results of piezoelectric shunted damping and energy harvesting popular single-degree-of-freedom-based models, transverse shear modal effective EMCC values are *very small* in particular for the first mode which is the common target of these applications.

Keywords: piezoceramic materials; shear response; modal effective electromechanical coupling coefficient; approximate evaluation; plane-strain; plane-stress; short-circuit; open-circuit; free-vibration; finite element

1. Introduction

Due to their inherent high material electromechanical coupling coefficients (Benjeddou 2007), shear-mode piezoceramic transducers have been often used during the last decade, in particular, for structural vibration shunted damping (Kim *et al.* 2005, Benjeddou and Ranger 2006, Trindade and Maio 2008, De Godoy and Trindade 2011, Dos Santos and Trindade 2011) and energy harvesting (Ren *et al.* 2010, Wang and Liu 2011, Zhao *et al.* 2012, Zhou *et al.* 2012). A key parameter for measuring or optimizing the latter applications performance is therefore the so-called (Deü and Benjeddou 2005) modal effective (*structural*) electromechanical coupling coefficient (EMCC).

*Corresponding author, Professor, E-mail: benjeddou@supmeca.fr

Indeed, as does the so-called (IEEE 1988) electromechanical coupling factor (EMCF) for a piezoelectric *material* undergoing a given *single-mode* response, the EMCC measures the amount of energy that can be converted from the *structural* vibration to the transducer electric one undergoing *multiple modes* response. Besides, as shown in (Trindade and Benjeddou 2009), it is a *non-dimensional* parameter that depends *approximately* on the transducer's piezoelectric *material* EMCF of its mode response and the *structural* ratio of the *open-circuit* (OC) *modal strain energy* (MSE) stored in the transducer to that of the piezoelectric adaptive structure (host + transducer). Thus, once the EMCF is fixed by the choice of the transducer's piezoelectric material, the modal effective EMCC depends only on the interaction between the piezoelectric transducer and its host. Therefore, its *accurate* numerical evaluation requires specific piezoelectric electromechanically coupled modal analyses under *short-circuit* (SC) and OC, considering the physical constraints of *equipotential* (EP) electrodes, electric boundary conditions (BC).

Nevertheless, *approximate* evaluations of the shear modal effective EMCC were proposed for their use with equivalent elastic modal analyses only; they use piezoelectric adaptive structures geometric and materials properties (Boudaoud *et al.* 2007, Majidi *et al.* 2010), modal SC (elastic) stiffness (Benjeddou 2006, Benjeddou and Ranger 2006, Benjeddou and Belouettar 2006), decoupled and coupled frequencies (Kim *et al.* 2005) or SC and OC elastic properties-induced frequencies (Benjeddou 2009, 2010). Some of these approximations were recently assessed numerically and experimentally for the piezoelectric *transverse-mode* response (Benjeddou 2014); in particular, the latter showed that the EMCC approximate evaluations do not see electro-mechanically *uncoupled* modes due to their incapacity to consider the physical EP constraints on the patch electrodes' nodal potential degrees of freedom (DOF). It is then a *first objective* of the present contribution to assess numerically, using three-dimensional (3D) coupled piezoelectric and elastic (with SC and OC transducer properties) finite element (FE) analyses, some of the modal effective EMCC approximate evaluations (Benjeddou 2014) for the piezoelectric *shear-mode* response of a typical cantilever sandwich beam benchmark (Benjeddou and Ranger 2006).

Single degree of freedom (SDOF) models are very popular for analyzing vibration shear piezoelectric shunted damping (Benjeddou and Ranger 2006) and energy harvesting (Aladwani *et al.* 2013, Zhao *et al.* 2012, Zhou *et al.* 2012). They provide high shear-mode performance for these applications. However, the MSE (Trindade and Maio 2008)– and 1D sandwich FE with EP constraints (Trindade and Benjeddou 2009)– based evaluations provided rather low shear-mode performance. This is due to an overestimation, by the SDOF models, of the shear strain energy stored in the transducer. Similarly, the *analytical* approximation of the OC electric condition by a nil electric displacement one (Deü and Benjeddou 2005, Boudaoud *et al.* 2007) provided a high shear modal effective EMCC while two-dimensional (2D) *plane-strain* (PStrain) and 3D piezoelectric coupled FE analysis, considering EP constraints on the electrodes nodal potential DOFs, showed lower or nil (Trindade and Benjeddou 2009) modal effective coupling performance. This is due to the fact that a nil electric displacement corresponds rather to a *non-electroded* (NE) condition while an electroded condition requires enforcing the EP physical constraints which effect averages the nodal electric potentials on the transducer electrodes, leading to the reduction of the shear strain energy stored in the transducer, hence reducing and even vanishing the resulting shear modal effective EMCC. A particular attention, within above first objective, will then be devoted to the 3D FE assessment of the EP constraints effect on the shear modal effective EMCC.

For computational cost efficiency and simplicity reasons, 2D PStrain and PStress analyses are often used for the analysis of shear-mode piezoelectric vibration (Baillargeon and Vel 2005a, Boudaoud *et al.* 2007, Majidi *et al.* 2010). Therefore, recent numerical and experimental

assessments (Benjeddou 2014) have shown that, for the piezoceramic materials transverse-mode vibration, it is better to use the PStress assumptions than PStrain ones. Moreover, it was proved that 3D SC and OC frequencies and resulting modal effective EMCC are bounded from below by PStress and from above by PStrain related results. It is then the *second objective* of the present work to check numerically the validity of these results for the piezoelectric shear-mode vibration.

The piezoelectric shear-mode has been used in a *unimorph* configuration (shear transducer surface-patched on a metallic cantilever beam) for structural vibration energy harvesting (Ren *et al.* 2010, Wang and Liu 2011, Zhao *et al.* 2012, Zhou *et al.* 2012) and in a *sandwich* configuration (shear patched core between metallic faces) for structural vibration shunted damping (Benjeddou and Ranger 2006, Trindade and Maio 2008, De Godoy and Trindade 2011, Dos Santos and Trindade 2011). A major difference between these two configurations is that the piezoceramic patches are transversely sheared by the elastic faces of the sandwich configuration; in this case, the *filling material* of the spaces not occupied by the piezoceramic patches plays a crucial role so that it renders using popular equivalent single layer (ESL) analytic (Abramovitch 2003, Ederly-Azulay and Abramovich 2006) and 1D FE (Manjunath and Bandyopadhyay 2006) beam models inadequate since they do not consider the deformation along the *width* direction and the faces relative displacements (shearing) against the core. A particular attention, within above two objectives, will then be devoted to the assessment of the filling material influence on shear-mode modal effective EMCC approximations and simplified 2D PStrain and PStress analyses.

Notice that the EP constraints and filling material Young modulus only influence on the shear modal effective EMCC was investigated in (Trindade and Benjeddou 2009) using 1D PStress-based sandwich beam FE and an MSE-based EMCC approximation; here, beside the EP constraints, different filling materials elastic and inertial properties are varied; they are assessed using 3D FE for a typical benchmark of a sandwich beam cantilever (Benjeddou and Ranger 2006) equivalent to the bimorph used for assessing numerically the transverse-mode (Benjeddou 2014).

In the following, the piezoelectric shear modal effective EMCC is first introduced, after the SC and OC free-vibration problems corresponding to the 3D piezoelectric shear-mode constitutive behavior, and its *approximate evaluations* are reviewed; then, simplified 2D PStrain and PStress piezoelectric constitutive behaviors of electroded shear piezoceramic patches are derived and corresponding expected SC and OC frequencies and resulting EMCC are discussed; next, a 3D FE assessment of different evaluation techniques of the shear modal effective EMCC is conducted, including the EP constraints effect; i.e., without (w/o) and with (w) EP (reference). Finally, 2D PStrain and PStress FE modal analyses are assessed under SC and OC electric conditions. For these numerical assessments, a cantilever sandwich beam benchmark from the piezoelectric shunted damping literature (Benjeddou and Ranger 2006) is used. It consists of two aluminum faces and a core embedding two separate shear piezoceramic patches and different filling materials, made of soft foam, hard foam (Baillargeon and Vel 2005b) and glue, for the non-occupied spaces. The cantilever shear piezoelectric adaptive sandwich beam benchmark is modeled using ANSYS[®] quadratic 2D (8 nodes quadrangular) and 3D (20 nodes hexahedral) piezoelectric and elastic FEs.

2. Approximate evaluations

This section aims first to derive the OC elastic matrix $[C^D]$ of a shear-mode *piezoceramic* patch that is polarized along its longer side and has electrodes covering its major surfaces that are

perpendicular to its thickness direction; the presence of these electrodes allows assuming a dominant *unidirectional* electric field (UDEFF) along the thickness direction so that the above OC elastic matrix can be reduced to $[\bar{C}^D]$. Then, the electromechanically coupled and uncoupled free-vibration problems associated to the host and adaptive structures with considering patch's SC and OC electric conditions in coupled modal analyses or having SC and OC elastic matrices only in uncoupled modal analyses. Finally, the frequencies resulting from the solutions of the different free-vibration problems are used for defining some approximate evaluations of the shear modal effective EMCC for its later numerical assessment.

2.1 Shear-mode constitutive equations

The electric *potential*-based piezoelectric FEs implement the *e-form* constitutive equations which write, in the 3D condensed matrix form, as

$$\begin{Bmatrix} \mathbf{T} \\ \mathbf{D} \end{Bmatrix} = \begin{bmatrix} \mathbf{C}^E & -\mathbf{e}^t \\ \mathbf{e} & \epsilon^S \end{bmatrix} \begin{Bmatrix} \mathbf{S} \\ \mathbf{E} \end{Bmatrix} \quad (1)$$

Where, superscript *t* denotes transpose operation; $\{\mathbf{T}\}$, $\{\mathbf{S}\}$, $\{\mathbf{D}\}$ and $\{\mathbf{E}\}$ are the mechanical stress and strain, and the electric displacement and field vectors; $[\mathbf{C}^E]$, $[\mathbf{e}]$ and $[\epsilon^S]$ are the SC (at constant electric field) elastic, stress piezoelectric and blocked (at constant strain) dielectric matrices.

For a nil *full* electric field, approximating a SC electric condition, the inverse constitutive equation (first line) of Eq. (1) reduces to the following SC purely elastic one

$$\{\mathbf{T}\} = [\mathbf{C}^E] \{\mathbf{S}\} \quad (2)$$

By condensing the electric field from Eq. (1), the latter transforms into an *h-form* as

$$\begin{Bmatrix} \mathbf{T} \\ \mathbf{E} \end{Bmatrix} = \begin{bmatrix} \mathbf{C}^D & -\mathbf{h}^t \\ -\mathbf{h} & \beta^S \end{bmatrix} \begin{Bmatrix} \mathbf{S} \\ \mathbf{D} \end{Bmatrix} \quad (3)$$

Where

$$[\mathbf{C}^D] = [\mathbf{C}^E] + [\mathbf{e}^t][\epsilon^S]^{-1}[\mathbf{e}], \quad [\mathbf{h}] = [\epsilon^S]^{-1}[\mathbf{e}], \quad [\beta^S] = [\epsilon^S]^{-1} \quad (4a, b, c)$$

This *h-form* is used in electrically *hybrid* FEs that use the dominant *unidirectional* electric displacement as an independent variable, for example for piezoelectric shunted damping analysis (De Godoy and Trindade 2011). It is also often used for formulating shunted damping (Kim *et al.* 2005) or energy harvesting (Zhou *et al.* 2012) analytical 1D models.

For a nil *full* electric displacement, approximating an OC electric condition, the inverse constitutive equation (first line) of Eq. (3) reduces to the following OC elastic one

$$\{\mathbf{T}\} = [\mathbf{C}^D] \{\mathbf{S}\} \quad (5)$$

Consider now the individual shear piezoceramic patch, shown in Fig. 1(a), which polarization lies along the material axis 3, while its electrodes cover the major surfaces lying in plane 2-3. Retaining the Voigt engineering notations and denoting C_{pq}^E ($p, q=1 \dots 6$) the SC elastic constants,

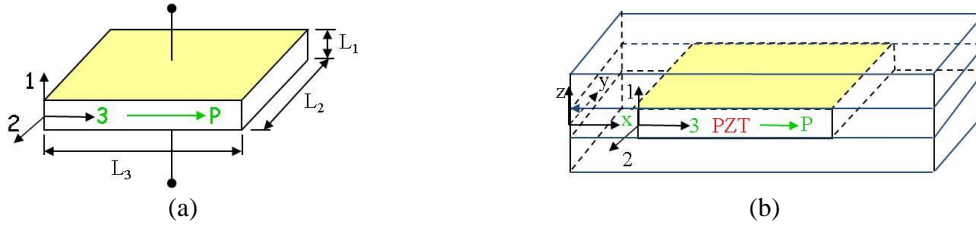


Fig. 1 Individual (a) and sandwiched (b) piezoceramic shear patch electroded on its major surfaces

e_{pk} ($k=1, 2, 3$) the stress piezoelectric constants and ϵ_{ii}^S ($i=1, 2, 3$) the blocked dielectric constants, the corresponding shear-mode piezoceramic (having *transverse isotropic* behavior) patch *e*-form 3D constitutive equations are explicitly

$$\begin{Bmatrix} T_1 \\ T_2 \\ T_3 \\ T_4 \\ T_5 \\ T_6 \end{Bmatrix} = \begin{bmatrix} C_{11}^E & C_{12}^E & C_{13}^E & 0 & 0 & 0 \\ C_{12}^E & C_{11}^E & C_{13}^E & 0 & 0 & 0 \\ C_{13}^E & C_{13}^E & C_{33}^E & 0 & 0 & 0 \\ \hline 0 & 0 & 0 & C_{55}^E & 0 & 0 \\ 0 & 0 & 0 & 0 & C_{55}^E & 0 \\ 0 & 0 & 0 & 0 & 0 & C_{66}^E = \frac{1}{2}(C_{11}^E - C_{12}^E) \end{bmatrix} \begin{Bmatrix} S_1 \\ S_2 \\ S_3 \\ S_4 \\ S_5 \\ S_6 \end{Bmatrix} - \begin{bmatrix} 0 & 0 & e_{31} \\ 0 & 0 & e_{31} \\ 0 & 0 & e_{33} \\ \hline 0 & e_{15} & 0 \\ e_{15} & 0 & 0 \\ 0 & 0 & 0 \end{bmatrix} \begin{Bmatrix} E_1 \\ E_2 \\ E_3 \end{Bmatrix} \quad (6a)$$

$$\begin{Bmatrix} D_1 \\ D_2 \\ D_3 \end{Bmatrix} = \begin{bmatrix} 0 & 0 & 0 & 0 & e_{15} & 0 \\ 0 & 0 & 0 & e_{15} & 0 & 0 \\ e_{31} & e_{31} & e_{33} & 0 & 0 & 0 \end{bmatrix} \begin{Bmatrix} S_1 \\ S_2 \\ S_3 \\ S_4 \\ S_5 \\ S_6 \end{Bmatrix} + \begin{bmatrix} \epsilon_{11}^S & 0 & 0 \\ 0 & \epsilon_{11}^S & 0 \\ 0 & 0 & \epsilon_{33}^S \end{bmatrix} \begin{Bmatrix} E_1 \\ E_2 \\ E_3 \end{Bmatrix} \quad (6b)$$

When the piezoceramic patch is used in a *sandwich* configuration and when the structural coordinate system is different from the material one, as in Fig. 1(b) and the present work, previous *e*-form constitutive equations should be transformed by interchanging the material constants subscript 3 to 1 and vice-versa; this leads, in the Cartesian coordinate system having axes x, y and z , to the following piezoceramic x - z shear-mode *e*-form 3D constitutive equations, where the electromechanical constants are those of Eqs. 6(a)-(b) and the stress and strain notations have been changed to σ_p, ϵ_q in order to differentiate them from the local ones T_p, S_q . Besides, 1, 2, 3, 4, 5, 6 Voigt subscripts denote now tensorial ones xx, yy, zz, yz, xz, xy

$$\begin{Bmatrix} \sigma_1 \\ \sigma_2 \\ \sigma_3 \\ \sigma_4 \\ \sigma_5 \\ \sigma_6 \end{Bmatrix} = \begin{bmatrix} C_{33}^E & C_{13}^E & C_{13}^E & 0 & 0 & 0 \\ C_{13}^E & C_{11}^E & C_{12}^E & 0 & 0 & 0 \\ C_{13}^E & C_{12}^E & C_{11}^E & 0 & 0 & 0 \\ \hline 0 & 0 & 0 & C_{66}^E = \frac{1}{2}(C_{11}^E - C_{12}^E) & 0 & 0 \\ 0 & 0 & 0 & 0 & C_{55}^E & 0 \\ 0 & 0 & 0 & 0 & 0 & C_{55}^E \end{bmatrix} \begin{Bmatrix} \epsilon_1 \\ \epsilon_2 \\ \epsilon_3 \\ \epsilon_4 \\ \epsilon_5 \\ \epsilon_6 \end{Bmatrix} - \begin{bmatrix} e_{33} & 0 & 0 \\ e_{31} & 0 & 0 \\ e_{31} & 0 & 0 \\ \hline 0 & 0 & 0 \\ 0 & 0 & e_{15} \\ 0 & e_{15} & 0 \end{bmatrix} \begin{Bmatrix} E_x \\ E_y \\ E_z \end{Bmatrix} \quad (7a)$$

$$\begin{Bmatrix} D_x \\ D_y \\ D_z \end{Bmatrix} = \begin{bmatrix} e_{33} & e_{31} & e_{31} & \cdots & 0 & 0 & 0 \\ 0 & 0 & 0 & \cdots & 0 & 0 & e_{15} \\ 0 & 0 & 0 & \cdots & 0 & e_{15} & 0 \end{bmatrix} \begin{Bmatrix} \varepsilon_1 \\ \varepsilon_2 \\ \varepsilon_3 \\ \varepsilon_4 \\ \varepsilon_5 \\ \varepsilon_6 \end{Bmatrix} + \begin{bmatrix} \varepsilon_{33}^S & 0 & 0 \\ 0 & \varepsilon_{11}^S & 0 \\ 0 & 0 & \varepsilon_{11}^S \end{bmatrix} \begin{Bmatrix} E_x \\ E_y \\ E_z \end{Bmatrix} \quad (7b)$$

With these matrices and Eq. 4(a), the *full* OC elastic matrix can be determined explicitly as

$$[C^D] = \begin{bmatrix} C_{33}^E + \frac{e_{33}^2}{\varepsilon_{33}^S} & C_{13}^E + \frac{e_{31}e_{33}}{\varepsilon_{33}^S} & C_{13}^E + \frac{e_{31}e_{33}}{\varepsilon_{33}^S} & \cdots & \cdots & \cdots & \cdots \\ & C_{11}^E + \frac{e_{31}^2}{\varepsilon_{33}^S} & C_{12}^E + \frac{e_{31}^2}{\varepsilon_{33}^S} & \cdots & \cdots & \cdots & \cdots \\ \text{sym.} & & C_{11}^E + \frac{e_{31}^2}{\varepsilon_{33}^S} & \cdots & \cdots & \cdots & \cdots \\ \cdots & \cdots & \cdots & C_{66}^E = \frac{1}{2}(C_{11}^E - C_{12}^E) & \cdots & \cdots & \cdots \\ \cdots & \cdots & \cdots & \cdots & C_{55}^E + \frac{e_{15}^2}{\varepsilon_{11}^S} & \cdots & \cdots \\ \cdots & \cdots & \cdots & \cdots & \cdots & C_{55}^E + \frac{e_{15}^2}{\varepsilon_{11}^S} & \cdots \end{bmatrix} \quad (8)$$

On the other hand, since the embedded shear-mode piezoceramic patch is electroded on its major surfaces, an UDEF along axis z can be assumed so that Eqs. 7(a)-(b) can be reduced to

$$\begin{Bmatrix} \sigma_1 \\ \sigma_2 \\ \sigma_3 \\ \sigma_4 \\ \sigma_5 \\ \sigma_6 \end{Bmatrix} = \begin{bmatrix} C_{33}^E & C_{13}^E & C_{13}^E & \cdots & 0 & 0 & 0 \\ C_{13}^E & C_{11}^E & C_{12}^E & \cdots & 0 & 0 & 0 \\ C_{13}^E & C_{12}^E & C_{11}^E & \cdots & 0 & 0 & 0 \\ \cdots & \cdots & \cdots & C_{66}^E = \frac{1}{2}(C_{11}^E - C_{12}^E) & 0 & 0 & 0 \\ 0 & 0 & 0 & 0 & C_{55}^E & 0 & 0 \\ 0 & 0 & 0 & 0 & 0 & C_{55}^E & 0 \end{bmatrix} \begin{Bmatrix} \varepsilon_1 \\ \varepsilon_2 \\ \varepsilon_3 \\ \varepsilon_4 \\ \varepsilon_5 \\ \varepsilon_6 \end{Bmatrix} - \begin{Bmatrix} 0 \\ 0 \\ 0 \\ 0 \\ e_{15} \\ 0 \end{Bmatrix} E_z \quad (9a)$$

$$\begin{Bmatrix} D_x \\ D_y \\ D_z \end{Bmatrix} = \begin{bmatrix} e_{33} & e_{31} & e_{31} & \cdots & 0 & 0 & 0 \\ 0 & 0 & 0 & \cdots & 0 & 0 & e_{15} \\ 0 & 0 & 0 & \cdots & 0 & e_{15} & 0 \end{bmatrix} \begin{Bmatrix} \varepsilon_1 \\ \varepsilon_2 \\ \varepsilon_3 \\ \varepsilon_4 \\ \varepsilon_5 \\ \varepsilon_6 \end{Bmatrix} + \begin{Bmatrix} 0 \\ 0 \\ 0 \end{Bmatrix} E_z \quad (9b)$$

Therefore, if the *transverse* electric field is nullified ($E_z=0$), as an approximation of the SC electric condition, Eq. 9(a) reduces to this *purely* elastic constitutive equation

$$\begin{Bmatrix} \sigma_1 \\ \sigma_2 \\ \sigma_3 \\ \sigma_4 \\ \sigma_5 \\ \sigma_6 \end{Bmatrix} = \begin{bmatrix} C_{33}^E & C_{13}^E & C_{13}^E & 0 & 0 & 0 \\ C_{13}^E & C_{11}^E & C_{12}^E & 0 & 0 & 0 \\ C_{13}^E & C_{12}^E & C_{11}^E & 0 & 0 & 0 \\ \hline 0 & 0 & 0 & C_{66}^E = \frac{1}{2}(C_{11}^E - C_{12}^E) & 0 & 0 \\ 0 & 0 & 0 & 0 & C_{55}^E & 0 \\ 0 & 0 & 0 & 0 & 0 & C_{55}^E \end{bmatrix} \begin{Bmatrix} \varepsilon_1 \\ \varepsilon_2 \\ \varepsilon_3 \\ \varepsilon_4 \\ \varepsilon_5 \\ \varepsilon_6 \end{Bmatrix} \quad \text{Or } \{\sigma\} = [C^E]\{\varepsilon\} \quad (10)$$

However, when the *transverse* electric displacement is nullified ($D_z=0$), as an approximation of the OC electric condition, this *reduced* OC elastic constitutive equation is obtained after condensing the transverse electric field (E_z) between Eqs. 9(a)-(b)

$$\begin{Bmatrix} \sigma_1 \\ \sigma_2 \\ \sigma_3 \\ \sigma_4 \\ \sigma_5 \\ \sigma_6 \end{Bmatrix} = \begin{bmatrix} C_{33}^E & C_{13}^E & C_{13}^E & 0 & 0 & 0 \\ C_{13}^E & C_{11}^E & C_{12}^E & 0 & 0 & 0 \\ C_{13}^E & C_{12}^E & C_{11}^E & 0 & 0 & 0 \\ \hline 0 & 0 & 0 & C_{66}^E = \frac{1}{2}(C_{11}^E - C_{12}^E) & 0 & 0 \\ 0 & 0 & 0 & 0 & C_{55}^E + \frac{e_{15}^2}{\epsilon_{11}^S} & 0 \\ 0 & 0 & 0 & 0 & 0 & C_{55}^E \end{bmatrix} \begin{Bmatrix} \varepsilon_1 \\ \varepsilon_2 \\ \varepsilon_3 \\ \varepsilon_4 \\ \varepsilon_5 \\ \varepsilon_6 \end{Bmatrix} \quad \text{Or } \{\sigma\} = [\bar{C}^D]\{\varepsilon\} \quad (11a)$$

Where, the OC x - z shear elastic constant can be also written in terms of the shear EMCF, k_{15} , as

$$C_{55}^D = C_{55}^E + \frac{e_{15}^2}{\epsilon_{11}^S} = \frac{C_{55}^E}{1 - k_{15}^2} \quad (11b)$$

From this relation, it can be concluded that, under a transverse UDEF assumption ($E_x=E_y=0$), the approximate OC condition ($D_z=0$) *stiffens* only the x - z shear elastic constant increasingly with the shear EMCF. Finally, the comparison with the *full* OC elastic matrix, as in Eq. (8), indicates that this *approximate* OC condition *filters* only the shear-mode response (longitudinal and transverse response modes are absent in Eq. (11)), while condensing all electric field components, that provides Eq. (8), modifies all the elastic constants, except *in-plane* shear one (C_{66}^E) so that the three response modes (longitudinal, transverse and shear) are present. Moreover, as can be seen from Eq. 9(b), the in-plane electric displacement components (D_x, D_y) are not nil under UDEF assumption; nevertheless, they do not enter into the electric energy contribution to the electromechanical enthalpy density, $H^* = \frac{1}{2} (\sigma_p \varepsilon_p - D_i E_i)$, $i=x, y, z$, since $D_\alpha E_\alpha=0$, $\alpha=x, y$. Besides, major surfaces electrodes, of area $A^\pm=A$ and outward normal $\vec{n} = \pm\vec{z}$, allow measuring electric charges from only the *transverse* electric displacement through this expression

$$Q = \frac{1}{2} \int_{A^\pm} \bar{D} \cdot \vec{n} \, dS = \int_A \bar{D}_z \, dS = \int_A D_z \, dS \quad (12)$$

Therefore, if the *transverse* electric displacement is *uniform* on the electrodes, an accurate OC electric condition ($Q=0$) is similar to approximating it by a nil *transverse* electric displacement ($D_z=0$). The latter assumption is often used in analytic modeling (Boudaoud *et al.* 2007). However, this is only true for NE case; thus, this approximation does not account for the physical EP constraints and leads to an overestimated modal effective EMCC (Trindade and Benjeddou 2009).

2.2 Free-vibration problems

For formulating a *potential*-based 3D FE model of a piezoceramic structure of total domain Ω ($=\Omega^{hs}$ of the host structure $+\Omega^p$ of piezoceramic transducers), materials *generic* mass density ρ (ρ_{hs} for host, ρ_p for piezoceramics) and in harmonic free-vibration of circular frequency ω , this piezoelectric-extended Lagrange functional (Benjeddou 2000) has to be made stationary ($\delta L=0$)

$$L = \frac{1}{2} \int_{\Omega^{hs}} \{\sigma\}^t \{\varepsilon\} d\Omega + \frac{1}{2} \int_{\Omega^p} (\{\sigma\}^t \{\varepsilon\} - \{E\}^t \{D\}) d\Omega - \frac{1}{2} \omega^2 \int_{\Omega} \{u\}^t \rho \{u\} d\Omega \quad (13)$$

Where, the first, second and third integral terms represent, respectively, the host elastic strain energy U , electromechanical enthalpy H and kinetic energy V ; the stress and electric displacement vectors are coupled to the strain and electric field ones through Eqs. 7(a)-(b).

For transducers *full* nil electric field (approximate SC) or displacement (approximate OC), the electromechanical enthalpy of the host (*hs*) plus piezoceramics reduces, respectively, to

$$H^E = \frac{1}{2} \int_{\Omega^{hs}} \{\varepsilon\}^t [C^{hs}] \{\varepsilon\} d\Omega + \frac{1}{2} \int_{\Omega^p} \{\varepsilon\}^t [C^E] \{\varepsilon\} d\Omega \quad (14a)$$

$$H^D = \frac{1}{2} \int_{\Omega^{hs}} \{\varepsilon\}^t [C^{hs}] \{\varepsilon\} d\Omega + \frac{1}{2} \int_{\Omega^p} \{\varepsilon\}^t [C^D] \{\varepsilon\} d\Omega \quad (14b)$$

Where, the OC (D) and SC (E) transducers elastic matrices are as in Eqs. (8), (10), respectively.

Under the UDEF assumption, the electromechanical enthalpy of the piezoceramics reduces to

$$\bar{H}^p = \frac{1}{2} \int_{\Omega^p} (\{\sigma\}^t \{\varepsilon\} - E_z D_z) d\Omega \quad (15a)$$

Where, the stress vector and *transverse* electric displacement are coupled to the strain vector and *transverse* electric field through the *reduced* constitutive equations, Eq. 9(a)-(b), that simplify to

$$\begin{Bmatrix} \sigma_1 \\ \sigma_2 \\ \sigma_3 \\ \sigma_4 \\ \sigma_6 \end{Bmatrix} = \begin{bmatrix} C_{33}^E & C_{13}^E & C_{13}^E & \vdots & 0 & 0 \\ C_{13}^E & C_{11}^E & C_{12}^E & \vdots & 0 & 0 \\ C_{13}^E & C_{12}^E & C_{11}^E & \vdots & 0 & 0 \\ \hdashline & \hdashline & \hdashline & C_{66}^E = \frac{1}{2}(C_{11}^E - C_{12}^E) & 0 & \\ 0 & 0 & 0 & \vdots & 0 & C_{55}^E \\ 0 & 0 & 0 & \vdots & 0 & \vdots \end{bmatrix} \begin{Bmatrix} \varepsilon_1 \\ \varepsilon_2 \\ \varepsilon_3 \\ \varepsilon_4 \\ \varepsilon_6 \end{Bmatrix} \quad \text{Or} \quad \{\bar{\sigma}\} = [\bar{C}^E] \{\bar{\varepsilon}\} \quad (15b)$$

$$\sigma_5 = C_{55}^E \varepsilon_5 - e_{15} E_z \quad (15c)$$

$$D_z = e_{15} \varepsilon_5 + \epsilon_{11}^S E_z \quad (15d)$$

Substituting Eqs. 15(b)-(d) into Eq. 15(a), transforms the latter to

$$\bar{H}^p = U_e^p - 2\bar{U}_m - \bar{U}_d \quad (16a)$$

Where the piezoceramics elastic, mutual and dielectric energies are defined by

$$U_e^p = \frac{1}{2} \int_{\Omega^p} (\{\bar{\varepsilon}\}^t [\bar{C}^E] \{\bar{\varepsilon}\} + C_{55}^E \varepsilon_5^2) d\Omega = \frac{1}{2} \int_{\Omega^p} \{\varepsilon\}^t [C^E] \{\varepsilon\} d\Omega, \quad (16b)$$

$$\bar{U}_m = \frac{1}{2} \int_{\Omega^p} e_{15} E_z \varepsilon_5 d\Omega, \quad \bar{U}_d = \frac{1}{2} \int_{\Omega^p} \varepsilon_{11}^S E_z^2 d\Omega \quad (16c, d)$$

Hence, for *approximate* SC ($E_z=0$) and OC ($D_z=0$) electric conditions and using Eqs. 15(c)-(d), the corresponding reduced electromechanical enthalpies (see Eq. (16)) become

$$\bar{H}^{pE} = U_e^p, \quad \bar{H}^{pD} = \bar{U}_e^{pD} \quad (17a)$$

With the approximate OC-*modified* elastic energy having this form

$$\bar{U}_e^{pD} = \frac{1}{2} \int_{\Omega^p} (\{\bar{\varepsilon}\}^t [\bar{C}^E] \{\bar{\varepsilon}\} + C_{55}^D \varepsilon_5^2) d\Omega = \frac{1}{2} \int_{\Omega^p} \{\varepsilon\}^t [\bar{C}^D] \{\varepsilon\} d\Omega \quad (17b)$$

And the piezoceramic reduced OC elastic matrix and OC-modified elastic x-z shear constant are given in Eq. 11(a) and (b), respectively.

Applying Ulitko's formula (Benjeddou 2010) to the adaptive structure with the piezoceramics under UDEF and with the help of Eqs (16b), (17b), (11b), the *quasi-static* effective EMCC is

$$\bar{K}_D^2 = \frac{\bar{H}^D - \bar{H}^E}{\bar{H}^D} = \frac{\bar{U}_e^{pD} - U_e^{pE}}{U_e^{hs} + \bar{U}_e^{pD}} = \frac{\frac{1}{2} \int_{\Omega^p} (C_{55}^D - C_{55}^E) \varepsilon_5^2 d\Omega}{\frac{1}{2} \int_{\Omega^{hs}} \{\varepsilon\}^t [C^{hs}] \{\varepsilon\} d\Omega + \frac{1}{2} \int_{\Omega^p} \{\varepsilon\}^t [\bar{C}^D] \{\varepsilon\} d\Omega} = k_{15}^2 \frac{\frac{1}{2} \int_{\Omega^p} C_{55}^D \varepsilon_5^2 d\Omega}{U_e^{hs} + \bar{U}_e^{pD}} \quad (18)$$

Since once the shear transducer piezoceramic material is chosen its shear properties (OC shear modulus $G_{xz}^D = C_{55}^D$ and EMCF k_{15}) are known, Eq. (18) shows that the *quasi-static* shear effective EMCC depends only on the *shear OC strain energy stored in the transducer*. Thus, the only way that remains for optimizing the shear effective EMCC is to optimize its size, particularly its polarization-side length-to-thickness ratio (Cao *et al.* 1998) and its position on the host structure (Trindade and Benjeddou 2009). Besides, Eq. (18) confirms the interpretation of its *modal* version proved in (Benjeddou and Trindade 2009, Benjeddou 2010), in the sense that the shear effective EMCC depends on the material shear EMCF and the strain energy fraction stored in the transducer.

In piezoelectric shunted damping (Benjeddou and Ranger 2006), the used EMCC definition has rather a SC (E) energy in the denominator of Eq. (18) leading to (after Eqs. (16b), (17b), (11b))

$$\bar{K}_E^2 = \frac{\bar{H}^D - \bar{H}^E}{\bar{H}^E} = \frac{\bar{U}_e^{pD} - U_e^{pE}}{U_e^{hs} + \bar{U}_e^{pE}} = \frac{\frac{1}{2} \int_{\Omega^p} (C_{55}^D - C_{55}^E) \varepsilon_5^2 d\Omega}{\frac{1}{2} \int_{\Omega^{hs}} \{\varepsilon\}^t [C^{hs}] \{\varepsilon\} d\Omega + \frac{1}{2} \int_{\Omega^p} \{\varepsilon\}^t [C^E] \{\varepsilon\} d\Omega} = \frac{k_{15}^2}{1 - k_{15}^2} \frac{\frac{1}{2} \int_{\Omega^p} C_{55}^E \varepsilon_5^2 d\Omega}{U_e^{hs} + U_e^p} \quad (19)$$

Compared to the expression at the end of Eq. (18), the last of Eq. (19) has the advantage to use only SC (E) properties; hence, it can be computed using purely elastic FEs. Nevertheless, it can be shown that both expressions are linked via these relations

$$\bar{K}_D^2 = \frac{\bar{K}_E^2}{1 + \bar{K}_E^2} \quad \text{or} \quad \bar{K}_E^2 = \frac{\bar{K}_D^2}{1 - \bar{K}_D^2} \quad (20)$$

Hence, since either Eq. (18) or (19) can be used for evaluating the quasi-static shear effective EMCC, the use of the SC (E) energy in the denominator is preferred. Notice that the shear quasi-static EMCC expressions, as in Eqs. (18)-(20), are *new*; they are *presented here for the first time*.

For FE assessment of the *modal* effective EMCC approximate evaluations, detailed in the subsequent sub-section, the following numerical modal analyses (see details in Benjeddou 2014) have to be conducted separately for the:

- *Host* structure, which discrete *elastic* free-vibration problem is

$$([K^{hs}] - \omega_{hs}^2 [M])\{U^{hs}\} = \{0\} \quad (21)$$

Where, $[K]$ and $[M]$ state for the stiffness and mass matrices. Here, foams replace transducers.

- *Adaptive* structure, which discrete *elastic* free-vibration problem, that uses the transducers' *full* SC (E) elastic matrix, is

$$([K^E] - \omega_E^2 [M])\{U^E\} = \{0\} \quad (22)$$

- *Adaptive* structure, which discrete *elastic* free-vibration problem, that uses the transducers' *full* OC (D) elastic matrix, is

$$([K^D] - \omega_D^2 [M])\{U^D\} = \{0\} \quad (23)$$

- *Adaptive* structure, which SC piezoelectric *coupled* discrete free-vibration problem is

$$([K^{SC}] - \omega_{SC}^2 [M])\{U^{SC}\} = \{0\} \quad (24)$$

- *Adaptive* structure under OC electric condition but *w/o* EP constraints (equivalent to a NE electric condition), which piezoelectric *coupled* discrete free-vibration problem is

$$([K^{NE}] - \omega_{NE}^2 [M])\{U^{NE}\} = \{0\} \quad (25)$$

- *Adaptive* structure under OC electric condition with EP constraints (reference solution), which piezoelectric *coupled* discrete free-vibration problem is

$$([K^{EP}] - \omega_{EP}^2 [M])\{U^{EP}\} = \{0\} \quad (26)$$

The frequencies resulting from the solutions of these six free-vibration problems, of which half of them (Eqs. (21)-(23)) are purely elastic and need only standard elastic FE modal analyses, will be used for post-processing the modal effective EMCC according to the hereafter presented different approximate and reference evaluation formulas.

2.3 Modal effective EMCC

An implementation of the shear modal effective EMCC, as given in Eq. (19), requires approximating the shear MSE stored in the piezoceramic transducers by the difference between the MSE of the adaptive sandwich structure with SC piezoceramics and the elastic host one only; the latter is considered here made of the elastic faces sandwiching a foam or glue core. Using *mass-normalized* modal shapes, the shear modal effective EMCC can be written in terms of the frequencies of the adaptive sandwich structure with SC piezoceramics, solution of Eq. (24), and those of the corresponding elastic host only, solution of Eq. (21), as follows

$$K_{15}^2 = \frac{k_{15}^2}{1 - k_{15}^2} \frac{f_{SC}^2 - f_{hs}^2}{f_{SC}^2} \tag{27}$$

It's worthy to mention that the numerator of the frequencies ratio can be *negative* although the shear modal effective EMCC should be *positive*; in this case, either an absolute value or simply squared maximum minus minimum over minimum values can be used (Benjeddou 2014). Hereafter, eventual negative sign presence is kept in order to detect the corresponding mode(s).

After solving the *elastic* free-vibration problems of Eqs. (22) and (23), that use *full* SC (*E*) and OC (*D*) *elastic* matrices of transducers, the modal effective EMCC can be approximated by

$$K_D^2 = \frac{f_D^2 - f_E^2}{f_E^2} \tag{28}$$

After solving the *coupled piezoelectric* free-vibration problems of Eqs. (24) and (25), the following expression can be used for evaluating the modal effective EMCC when the electrodes physical EP constraints are *not enforced* during the OC modal analysis for solving Eq. (25)

$$K_{NE}^2 = \frac{f_{NE}^2 - f_{SC}^2}{f_{SC}^2} \tag{29}$$

Finally, the solutions of the *coupled piezoelectric* free-vibration problems of Eqs. (24) and (26) allow the following *reference* evaluation of the modal effective EMCC when the electrodes physical EP constraints are *enforced* during the OC modal analysis for solving Eq. (26)

$$K_{EP}^2 = \frac{f_{EP}^2 - f_{SC}^2}{f_{SC}^2} \tag{30}$$

Notice that shear subscripts '15' have been used only for the modal effective EMCC in Eq. (27) because this approximation uses explicitly the shear modal EMCF k_{15} . However, the other two approximations by Eqs. (28) and (29) and by the reference evaluation of Eq. (30) provide a modal effective EMCC that may involve not only the shear modal EMCF but also the longitudinal k_{33} and transverse k_{31} EMCF; i.e., evaluations (28)-(30) consider *multimode* responses, while Eq. (27) can be seen as a *single-mode* (shear) response (*approximate*) evaluation. The three approximate evaluations of Eq. (27)-(29) will be later numerically assessed against the reference one of Eq. (30).

3. Simplified analyses

All commercial FE codes use a PStrain/PStress 2D work plane lying in the global coordinate system plane x - y . Therefore, since the shear piezoceramic patches to be used here are poled along their length, the polarization remains then as in the 3D case (Fig. 1(b)) parallel to the x -axis (Fig. 2).

Therefore, the 3D e-form constitutive equations, as in Eqs. 7(a)-(b), can be used as a starting point of their reduction to the x - y 2D work plane. The first reduction step is common to both PStrain and PStress models; it assumes a dominant UDEF along the y axis since the major surfaces electrodes are now perpendicular to the latter direction (see orange lines in Fig. 2); i.e.

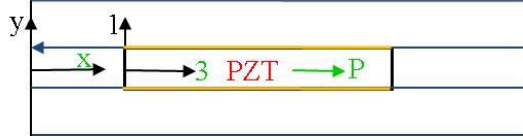


Fig. 2 FE 2D modeling plane of a sandwiched major surfaces electroded shear piezoceramic transducer

$$E_x = E_z = 0 \quad (31)$$

This assumption reduces the 3D e -form constitutive equations, as in Eqs. 7(a)-(b), to

$$\begin{Bmatrix} \sigma_1 \\ \sigma_2 \\ \sigma_3 \\ \sigma_4 \\ \sigma_5 \\ \sigma_6 \end{Bmatrix} = \begin{bmatrix} C_{33}^E & C_{13}^E & C_{13}^E & \dots & 0 & 0 & 0 \\ C_{13}^E & C_{11}^E & C_{12}^E & \dots & 0 & 0 & 0 \\ C_{13}^E & C_{12}^E & C_{11}^E & \dots & 0 & 0 & 0 \\ \dots & \dots & \dots & \dots & C_{66}^E = \frac{1}{2}(C_{11}^E - C_{12}^E) & 0 & 0 \\ 0 & 0 & 0 & \dots & 0 & C_{55}^E & 0 \\ 0 & 0 & 0 & \dots & 0 & 0 & C_{55}^E \end{bmatrix} \begin{Bmatrix} \varepsilon_1 \\ \varepsilon_2 \\ \varepsilon_3 \\ \varepsilon_4 \\ \varepsilon_5 \\ \varepsilon_6 \end{Bmatrix} - \begin{Bmatrix} 0 \\ 0 \\ 0 \\ 0 \\ 0 \\ e_{15} \end{Bmatrix} E_y \quad (32a)$$

$$\begin{Bmatrix} D_x \\ D_y \\ D_z \end{Bmatrix} = \begin{bmatrix} e_{33} & e_{31} & e_{31} & \dots & 0 & 0 & 0 \\ 0 & 0 & 0 & \dots & 0 & 0 & e_{15} \\ 0 & 0 & 0 & \dots & 0 & e_{15} & 0 \end{bmatrix} \begin{Bmatrix} \varepsilon_1 \\ \varepsilon_2 \\ \varepsilon_3 \\ \varepsilon_4 \\ \varepsilon_5 \\ \varepsilon_6 \end{Bmatrix} + \begin{Bmatrix} 0 \\ \epsilon_{11}^S \\ 0 \end{Bmatrix} E_y \quad (32b)$$

These equations can also be re-written so that to isolate the electromechanically coupled ones

$$\begin{Bmatrix} \sigma_1 \\ \sigma_2 \\ \sigma_3 \\ \sigma_4 \\ \sigma_5 \end{Bmatrix} = \begin{bmatrix} C_{33}^E & C_{13}^E & C_{13}^E & \dots & 0 & 0 \\ C_{13}^E & C_{11}^E & C_{12}^E & \dots & 0 & 0 \\ C_{13}^E & C_{12}^E & C_{11}^E & \dots & 0 & 0 \\ \dots & \dots & \dots & \dots & C_{66}^E = \frac{1}{2}(C_{11}^E - C_{12}^E) & 0 \\ 0 & 0 & 0 & \dots & 0 & C_{55}^E \end{bmatrix} \begin{Bmatrix} \varepsilon_1 \\ \varepsilon_2 \\ \varepsilon_3 \\ \varepsilon_4 \\ \varepsilon_5 \end{Bmatrix} \quad \text{Or} \quad \{\bar{\sigma}\} = [\bar{C}_{2D}^E] \{\bar{\varepsilon}\} \quad (33a)$$

$$\sigma_6 = C_{55}^E \varepsilon_6 - e_{15} E_y \quad (33b)$$

$$D_y = e_{15} \varepsilon_6 + \epsilon_{11}^S E_y \quad (33c)$$

Notice that the piezoelectric shear response in hand is now an in-plane (x - y) one. Also, Eqs. 33(a-c) allow using the same quasi-static shear effective EMCC evaluations as in Eq. (18)-(19), provided that ε_6 replaces ε_5 and 2D PStrain/PSress domain integrals are handled adequately.

3.1 Plane strain behaviors

PStrain behavior results here from assuming nil transverse (to the work plane) strains; that is

$$\varepsilon_3 = \varepsilon_4 = \varepsilon_5 = 0 \tag{34}$$

While Eqs. 33(b)-(c) are not affected by these relations, substituting the latter in Eq. 33(a) reduces it, after removing its last three lines and columns, to

$$\begin{Bmatrix} \sigma_1 \\ \sigma_2 \end{Bmatrix} = \begin{bmatrix} C_{33}^E & C_{13}^E \\ C_{13}^E & C_{11}^E \end{bmatrix} \begin{Bmatrix} \varepsilon_1 \\ \varepsilon_2 \end{Bmatrix} \tag{35}$$

Notice that although the transverse normal stress is not nil ($\sigma_3 = C_{13}^E \varepsilon_1 + C_{12}^E \varepsilon_2$), its product with the dual transverse normal strain is nil; hence, it does not intervene in the 2D variational formulation (VF) and related 2D FE one. For this reason, this stress component is dropped hereafter. Therefore, the 2D PStrain constitutive behavior is defined by Eqs. (35) and 33(b)-(c); these equations can be also written in this electromechanical condensed matrix form

$$\begin{Bmatrix} \sigma_1 \\ \sigma_2 \\ \sigma_6 \\ D_y \end{Bmatrix} = \begin{bmatrix} C_{33}^E & C_{13}^E & 0 & 0 \\ C_{13}^E & C_{11}^E & 0 & 0 \\ 0 & 0 & C_{55}^E & -e_{15} \\ 0 & 0 & e_{15} & \epsilon_{11}^S \end{bmatrix} \begin{Bmatrix} \varepsilon_1 \\ \varepsilon_2 \\ \varepsilon_6 \\ E_y \end{Bmatrix} \tag{36}$$

Under a nil electric field ($E_y=0$), approximating a SC electric condition, Eq. (36) reduces to

$$\begin{Bmatrix} \sigma_1 \\ \sigma_2 \\ \sigma_6 \end{Bmatrix} = \begin{bmatrix} C_{33}^E & C_{13}^E & 0 \\ C_{13}^E & C_{11}^E & 0 \\ 0 & 0 & C_{55}^E \end{bmatrix} \begin{Bmatrix} \varepsilon_1 \\ \varepsilon_2 \\ \varepsilon_6 \end{Bmatrix} \tag{37}$$

Notice that the transverse electric displacement is not nil ($D_y=e_{15}\varepsilon_6$) but does not intervene in the approximate SC 2D PStrain VF and related FE one, since its product with the electric field is nil; however, it can be post-treated and used for computing the electric charges produced on the electrodes of the transducer which can be seen here as a *charge sensor*

$$Q_{2D} = \int_x D_y \, dx = \int_x e_{15} \varepsilon_6 \, dx \tag{38}$$

When the electric displacement is now considered nil ($D_y=0$) as an approximation of the OC electric condition, the electric field can be condensed between Eqs. 33(b)-(c) so that an approximate OC-modified shear elastic constant, as in Eq. (11b), is obtained; grouping the modified Eq. 33(a) with Eq. (35) provides these approximate OC constitutive equations

$$\begin{Bmatrix} \sigma_1 \\ \sigma_2 \\ \sigma_6 \end{Bmatrix} = \begin{bmatrix} C_{33}^E & C_{13}^E & 0 \\ C_{13}^E & C_{11}^E & 0 \\ 0 & 0 & C_{55}^D \end{bmatrix} \begin{Bmatrix} \varepsilon_1 \\ \varepsilon_2 \\ \varepsilon_6 \end{Bmatrix} \tag{39}$$

Where, here, the electric field is not nil ($E_y = -\frac{e_{15}}{\epsilon_{11}} \epsilon_6$) but does not intervene in the approximate OC 2D PStrain VF and related FE one, since its product with the electric displacement is nil; however, it can be post-treated and used for quantifying the electric potential produced between the electrodes of the transducer which can be seen here as a *potential sensor*.

$$\varphi_{2D} = -\int_y E_y dy = \int_y \frac{e_{15}}{\epsilon_{11}} \epsilon_6 dy \quad (40)$$

From Eqs. (37) and (39), it is clear that the SC electric condition provides a purely elastic 2D PStrain constitutive behavior, while the OC one leads to the same elastic behavior but with a modified shear elastic constant (as in Eq. 11(b)) only.

3.2 Plane stress behaviors

PStress behavior results here from assuming nil transverse (to the work plane) stresses; that is

$$\sigma_3 = \sigma_4 = \sigma_5 = 0 \quad (41)$$

While Eqs. 33(b)-(c) are also not affected here by these relations, substituting the latter in Eqs. 33(a) provides nil transverse shear strains ($\epsilon_4=\epsilon_5=0$) but a non-nil transverse normal strain

$$\epsilon_3 = -\frac{1}{C_{11}^E} (C_{13}^E \epsilon_1 + C_{12}^E \epsilon_2) \quad (42)$$

Substituting back this relation into the first two lines of Eq. 33(a) reduces the latter to

$$\begin{Bmatrix} \sigma_1 \\ \sigma_2 \end{Bmatrix} = \begin{bmatrix} \bar{C}_{33}^E & \bar{C}_{13}^E \\ \bar{C}_{13}^E & \bar{C}_{11}^E \end{bmatrix} \begin{Bmatrix} \epsilon_1 \\ \epsilon_2 \end{Bmatrix} \quad (43a)$$

Where

$$\bar{C}_{11}^E = C_{11}^E - \frac{(C_{12}^E)^2}{C_{11}^E}, \quad \bar{C}_{13}^E = C_{13}^E - \frac{C_{13}^E C_{12}^E}{C_{11}^E}, \quad \bar{C}_{33}^E = C_{33}^E - \frac{(C_{13}^E)^2}{C_{11}^E} \quad (43b)$$

Notice that although the transverse normal strain is not nil (see Eq. (42)), its product with the dual transverse normal stress is nil; hence, it does not intervene in the 2D VF and related 2D FE one. For this reason, this strain component is dropped hereafter. Therefore, the 2D PStress constitutive behavior is defined by Eqs. (43) and 33(b)-(c); these equations can be also written in this electromechanical condensed matrix form

$$\begin{Bmatrix} \sigma_1 \\ \sigma_2 \\ \sigma_6 \\ D_y \end{Bmatrix} = \begin{bmatrix} \bar{C}_{33}^E & \bar{C}_{13}^E & 0 & 0 \\ \bar{C}_{13}^E & \bar{C}_{11}^E & 0 & 0 \\ 0 & 0 & C_{55}^E & -e_{15} \\ 0 & 0 & e_{15} & \epsilon_{11}^S \end{bmatrix} \begin{Bmatrix} \epsilon_1 \\ \epsilon_2 \\ \epsilon_6 \\ E_y \end{Bmatrix} \quad (44)$$

Under a nil electric field ($E_y=0$), approximating a SC electric condition, Eq. (44) reduces to

$$\begin{Bmatrix} \sigma_1 \\ \sigma_2 \\ \sigma_6 \end{Bmatrix} = \begin{bmatrix} \bar{C}_{33}^E & \bar{C}_{13}^E & 0 \\ \bar{C}_{13}^E & \bar{C}_{11}^E & 0 \\ 0 & 0 & C_{55}^E \end{bmatrix} \begin{Bmatrix} \epsilon_1 \\ \epsilon_2 \\ \epsilon_6 \end{Bmatrix} \quad (45)$$

Notice that the transverse electric displacement is again not nil ($D_y=e_{15}\epsilon_6$) but does not intervene in the approximate SC 2D PStress VF and related FE one, since its product with the electric field is nil; however, it can be post-treated and used for computing the electric charges produced on the electrodes (see Eq. (38)) of the transducer which is a *charge sensor*.

When the electric displacement is now considered nil ($D_y=0$) as an approximation of the OC electric condition, the electric field can be condensed between Eqs. 33(b)-(c) so that an approximate OC-modified shear elastic constant, as in Eq. (11b), is obtained; grouping the modified Eq. 33(a) with Eq. 43(a) provides these PStress approximate OC constitutive equations

$$\begin{Bmatrix} \sigma_1 \\ \sigma_2 \\ \sigma_6 \end{Bmatrix} = \begin{bmatrix} \bar{C}_{33}^E & \bar{C}_{13}^E & 0 \\ \bar{C}_{13}^E & \bar{C}_{11}^E & 0 \\ 0 & 0 & C_{55}^D \end{bmatrix} \begin{Bmatrix} \epsilon_1 \\ \epsilon_2 \\ \epsilon_6 \end{Bmatrix} \tag{46}$$

Where, here also, the electric field is not nil ($E_y = -\frac{e_{15}}{\epsilon_{11}} \epsilon_6$) but does not intervene in the approximate OC 2D PStress VF and related FE one since its product with the electric displacement is nil; however, it can be post-treated and used for quantifying the electric potential between the electrodes (see Eq. (40)) of the transducer which is here also a *potential sensor*.

From Eqs. (45)-(46), it is clear that the SC electric condition provides a purely elastic 2D PStress constitutive behavior, while the OC one leads to the same elastic behavior but with a modified shear elastic constant (as in Eq. 11(b)) only.

3.3 Expected responses

The 3D *potential*-displacement VF, retained for formulating commercial coupled piezoelectric FE harmonic free-vibration analysis of an adaptive structure, results from vanishing the virtual variation of the extended Lagrange functional of Eq. (13) so that this *indicial* form is obtained

$$\int_{\Omega} \delta \epsilon_p \sigma_p d\Omega - \int_{\Omega^p} \delta E_i D_i d\Omega - \omega^2 \int_{\Omega} \delta u_i \rho u_i d\Omega = 0 \tag{47}$$

Where, the stresses and electric displacements are related to strains and electric fields via Eq. (7).

In order to use 3D SC (E), Eq. (7a), and *full* OC (D), Eq. (8), elastic properties for corresponding *approximate* SC (Eq. (22)) and OC (Eq. (23)) modal analyses, Eq. (47) is reduced to

$$\int_{\Omega} \delta \epsilon_p \sigma_p d\Omega - \omega^2 \int_{\Omega} \delta u_i \rho u_i d\Omega = 0 \tag{48}$$

Notice that Eq. (48) is also used for host structure free-vibration analysis via solving Eq. (21).

However, since either *transverse* strains or stresses and *in-plane* electric fields vanish under 2D UDEF, PStrain and PStress assumptions, Eq. (47) reduces to

$$\int_{\Omega} (\delta \epsilon_{\alpha} \sigma_{\alpha} + \delta \epsilon_6 \sigma_6) d\Omega - \int_{\Omega^p} \delta E_y D_y d\Omega - \omega^2 \int_{\Omega} \delta u_{\alpha} \rho u_{\alpha} d\Omega = 0 \tag{49}$$

Where, *in-plane* stresses and *transverse* electric displacement are related to *in-plane* strains and *transverse* electric field via Eqs. (36) and (44) for PStrain and PStress analyses, respectively.

However, for *approximate* SC ($E_y=0$) and OC ($D_y=0$) free-vibration analyses, the middle integral term of Eq. (49) vanishes, leading to this classical 2D elastic VF

$$\int_{\Omega} (\delta \varepsilon_{\alpha} \sigma_{\alpha} + \delta \varepsilon_{\sigma} \sigma_{\sigma}) d\Omega - \omega^2 \int_{\Omega} \delta u_{\alpha} \rho u_{\alpha} d\Omega = 0 \quad (50)$$

Where, in-plane stresses are related to their dual strains via elastic Eqs. (37) and (39) for SC and OC PStrain analyses and Eqs. (45)-(46) for SC and OC PStress ones.

As the electric conditions (SC or OC) do not influence the inertial term, the corresponding frequencies resulting from solving electromechanically coupled 3D and 2D VF and related free-vibration problems will be influenced only by the elastic stiffness parameters. In fact, the EP condition is also an important factor but its global influence cannot be predicted from the local constitutive behaviors. Therefore, it is expected that:

- SC conditions do not affect much piezoelectric structures modal analysis; thus, using transducers SC (E) elastic matrix of Eq. (10) within purely elastic or electromechanically coupled FE free-vibration analysis should provide *similar* frequencies;

- Use of *full* OC (D) elastic matrix of Eq. (8) within a purely elastic FE modal analysis should provide *close or similar* frequencies to those resulting from coupled piezoelectric one under OC conditions but w/o EP constraints (denoted here NE);

- Use of the EP constraints for OC coupled piezoelectric FE modal analysis should provide *lower* frequencies, hence lower modal effective EMCC, than those from NE (w/o EP) coupled or OC modified elastic properties – based modal analyses. Also, for electrodes *asymmetrically* distributed transverse electric displacement, EP constraints should have the effect to *cancel* produced electric charges as can be seen from Eq. (38) for the 2D analysis; this shall result in electromechanically *uncoupled* corresponding modes;

- Either from 3D or 2D modal analysis, OC frequencies are expected to be higher than SC ones; this is due to the *stiffening* effect of OC conditions as can be seen from Eqs. (8) and (11).

- Frequencies resulting from UDEF 2D PStress-based FE modal simplified analysis should be *lower* than those from 3D and from UDEF 2D PStrain-based ones. As can be seen from Eq. 43(b), this is due to the PStress *decreased* elastic constants. Hence, the same shall happen for the resulting shear modal effective EMCC;

- UDEF assumption influence on the OC piezoelectric behavior is limited to the transverse shear (*x-z* for 3D, *x-y* for 2D) elastic constant *modification* only, as can be seen from Eq. (11). Hence, *approximate* OC frequencies should differ only *slightly* from SC ones, leading to *low* modal shear effective EMCC. Indeed, as can be seen from the latter's approximation by Eqs. (18)-(19), the performance will depend only on the shear MSE stored in the transducers when their positions, dimensions, transverse shear elastic constant and EMCF are known.

These predictions from the shear modal effective EMCC approximate evaluations and UDEF 2D PStrain and PStress simplified analyses shall be numerically assessed in the subsequent section.

4. Numerical assessment

For a typical shear piezoceramic sandwich cantilever beam benchmark, adapted from (Benjeddou and Ranger 2006), this section aims to assess numerically the: (i) performance of shear modal effective EMCC approximate evaluations requiring sandwich host (whole core made of transducers space filling material) and SC adaptive sandwich structure frequencies (Eq. (27)), and SC (E) and OC (E) transducers' elastic properties-induced ones (Eq. (28)); (ii) EP constraints influence on the modal effective EMCC evaluation with NE (w/o EP) conditions (Eq. (29)); (iii)

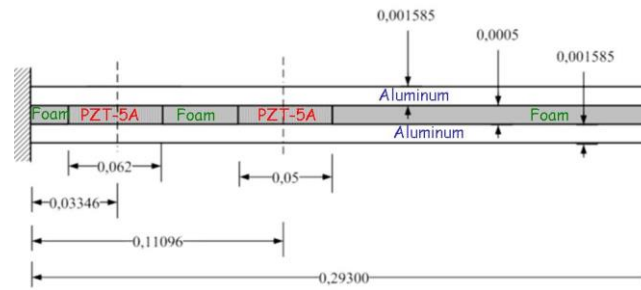


Fig. 3 2D sketch of the shear piezoceramic sandwich cantilever beam benchmark (dimensions in mm)

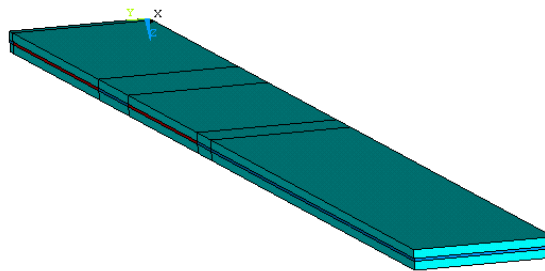


Fig. 4 3D geometric model of the shear piezoceramic sandwich cantilever beam benchmark

shear modal effective EMCC reference evaluation (uses OC with EP constraints) using modal UDEF 2D PStrain and PStress simplified analyses; (iv) sandwich core filling material of the transducers spaces influence on the shear modal effective EMCC approximate evaluations and its UDEF 2D PStrain and PStress simplified analyses.

4.1 Shear-mode benchmark and models

For the numerical (FE) assessment of the shear modal effective EMCC approximate evaluations and simplified analyses, the benchmark proposed earlier for shear piezoelectric shunted damping numerical evaluation (Benjeddou and Ranger 2006) is adapted as in Fig. 3. It consists of a sandwich cantilever beam with aluminum faces and hybrid core made of filling material and two piezoceramic (PZT-5A) patches which polarization is along the beam length. The patches are covered on their major surfaces with electrodes perpendicular to their thickness direction so that they work in the shear-mode response. They have the same thickness (2.55 cm) as the host beam. Three materials, made of soft foam, hard foam and glue, are considered for filling the core spaces non-occupied by the transducers. Materials properties are given in the Appendix.

The corresponding 3D geometric model was generated within ANSYS[®] by connecting key points of Fig. 3 sections in order to get lines, from which areas are created; the latter were then extruded in the width direction in order to create the volumes shown in Fig. 4. This simple basic procedure helps automatic enforcing the interfacial nodes coincidence during the FE mesh phase.

ANSYS[®] SOLID5 element has been used for the FE mesh. It has three displacement translations (U_x , U_y , U_z) as nodal DOFs for elastic analyses; these are augmented by the *electric potential* (VOLT) as a fourth nodal DOF for SC and OC, with or without (NE) EP constraints enforcing, piezoelectric coupled analyses. Each patch was meshed using 3 FEs along thickness

Table 1 First six x - z bending modes frequencies of the adaptive sandwich beam with *soft foam* filled spaces

x - z bending modes	f_{hs} (Hz)	f_E (Hz)	f_{SC} (Hz)	f_{EP} (Hz)	f_{NE} (Hz)	f_D (Hz)
1	36.443	37.483	37.483	37.484	37.487	37.513
2	191.87	213.21	213.21	213.23	213.26	213.35
3	461.72	538.38	538.38	538.44	538.57	538.78
4	795.4	972.59	972.6	972.82	972.91	973.15
5	1200.5	1434.7	1434.7	1434.9	1435.7	1436.4
6	1683.9	2101	2101	2101.1	2103	2104.5

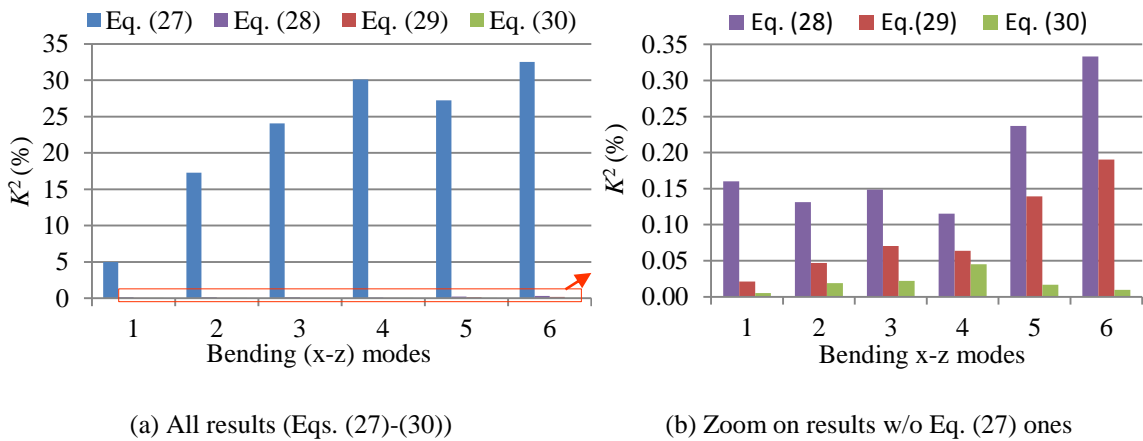
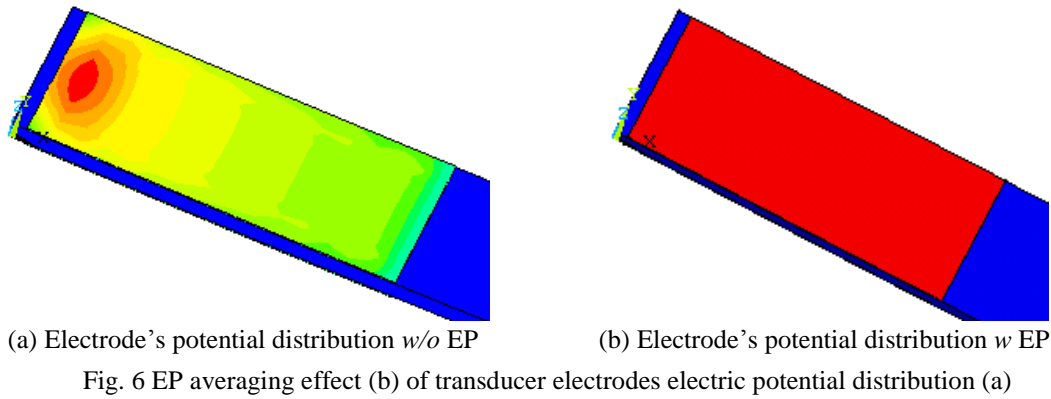
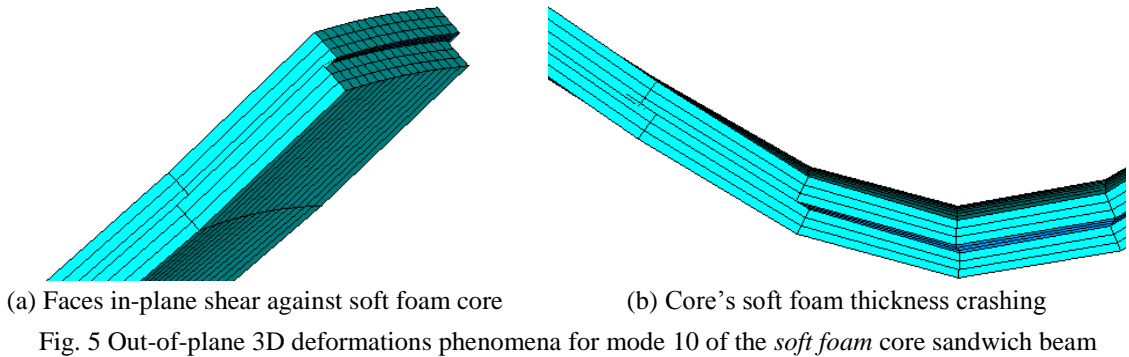
and 15 ones along in-plane sides, while each face was meshed with $69 \times 15 \times 3$ FEs along x , y and z directions, resulting in an adaptive sandwich hexahedral *mapped mesh* of 9315 FEs. For SC modal analyses, all electrodes have imposed nil electric potential, while for OC ones, the electric DOFs are coupled when EP constraints are enforced, but let free when they are not (NE condition). The 2D FE models, lying mandatory in the x - y plane with y -axis being in the thickness direction, have the same mesh as that of the 3D length-thickness plane.

4.2 Approximate evaluations

This sub-section assesses the shear modal effective EMCC approximate evaluations using Eqs. (27)-(29) against the reference (Eq. (30)) through 3D elastic and coupled piezoelectric FE modal analyses of above shear sandwich cantilever beam benchmark; only the first ten 3D modes characterizing *beam-like modal shapes* are retained; this leads to the first six x - z bending modes.

The frequency results corresponding to the *soft foam* filling material case are given in Table 1. They show that host structure frequencies are *lower* than adaptive structure ones; this is due to the core *softness*. Interesting is the observed *identical* f_{SC} (coupled piezoelectric computations – induced) and f_E (elastic computations – induced) values. Table 1 5th and 6th columns comparison indicates that EP constraints have the effect to *decrease* OC frequencies. Also, frequencies resulting from using *full* (f_D) elastic properties *overestimate* OC (EP, NE) ones. All these observations confirm the frequency predictions made in above expected results section.

From modal shapes visualizations, it was noticed that the bending modes computed order of the host structure (1, 2, **5**, 6, **8**, 10) is different from that (1, 2, **4**, 6, **9**, 10) of the adaptive structures with SC, OC (EP, NE) electrodes and with the patches having elastic properties under constant electric fields (E) only, while the modes computed using the patches properties with constant electric displacements (full D) have another order (1, 2, **4**, 6, **8**, 10). Hence, care should be taken since the 3D FE modes order is shown to depend on the analyzed configuration. Here, this concerns the 3rd and 5th x - z bending modes (in bold in Table 1) which have to be identified carefully from the 3D FE computed modal shapes. Another important observation is that the electric conditions (SC, EP, NE) do not influence the modes order. The same order as the latter is obtained when simulating the adaptive structure with only the patches elastic properties under constant electric fields (E). However, care should be taken when replacing the patches properties by the filling materials ones (host structure case) and when using constant electric displacements (full D). The visualizations show also local 3D foam effects like ‘in-plane shear’, as in Fig. 5(a), that is due to the faces’ relative displacements along the width direction against the core, or the foam ‘thickness crushing’ as in Fig. 5(b); these effects appear first at the second mode but become



crucial starting from the third mode. These out-of-working plane 3D phenomena cannot be caught by ESL and sandwich 1D beam, 2D PStrain or PStress and SDOF models.

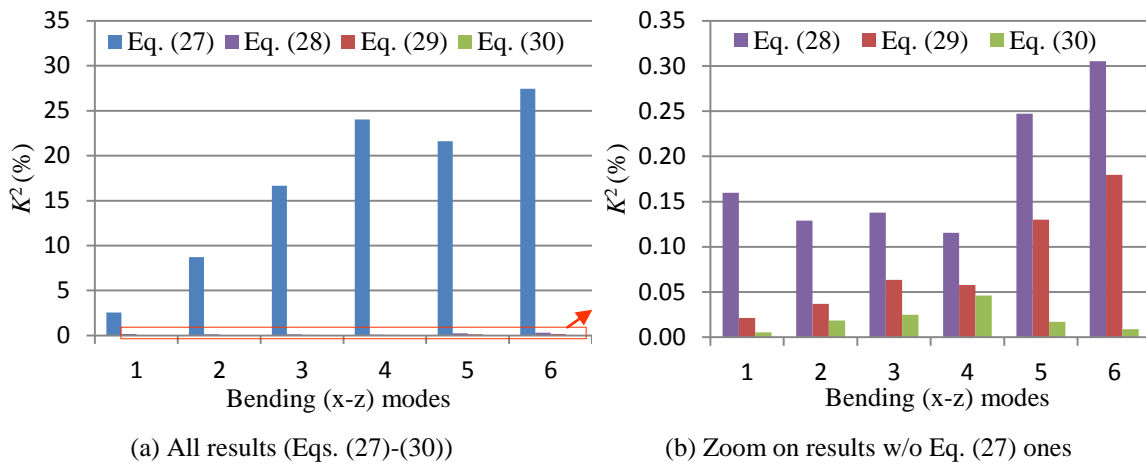
The EP averaging effect of the electrode's electric potential non-uniform distribution when these constraints are not enforced is also illustrated in Fig. 6.

Shear modal effective EMCCs, post-treated from frequencies of Table 1, are shown in Fig. 7.

Fig. 7(a) indicates clearly that the approximate evaluation by Eq. (27) overestimates greatly the

Table 2 First six x - z bending modes frequencies of the adaptive sandwich beam with *hard foam* filled spaces

x - z bending modes	f_{hs} (Hz)	f_E (Hz)	f_{SC} (Hz)	f_{EP} (Hz)	f_{NE} (Hz)	f_D (Hz)
1	37.06	37.594	37.594	37.595	37.598	37.624
2	206.56	217.25	217.25	217.27	217.29	217.39
3	511.83	566.38	566.38	566.45	566.56	566.77
4	892.32	1040.4	1040.4	1040.6	1040.7	1041
5	1342	1537.3	1537.3	1537.4	1538.3	1539.2
6	1863.2	2229.9	2229.9	2230	2231.9	2233.3

Fig. 8 Shear modal effective EMCC of the sandwich beam with *hard foam* as filling material

reference one (Eq. (30)) and is much higher than that by the other approximations (Eqs. (28)-(29)). However, its results are in line with those obtained using 1D hybrid sandwich/ESL beam FE and modal stiffness (instead of frequency) ratio-based approximation for the shear piezoceramic shunted damping evaluation (Benjeddou and Ranger 2006), where obtained shear modal effective EMCCs were excessively promising (10 times higher) compared to reference (Eq. (30)) ones. The latter and approximate (Eq. (28)-(29)) evaluations show clearly (Fig. 7(b)) that the shear modal effective EMCC is *very low*, predicting a *low* performance of vibration shear piezoceramic shunted damping (Trindade and Maio 2008) and energy harvesting applications. Fig. 7(b) shows also that, while the reference (Eq. (30)) evaluation shows an *optimum* modal effective EMCC value (for mode 4), approximate (Eqs. (28)-(29)) ones provide *increasing* modal effective EMCC values with *increasing* modes order. Besides, comparison of the latter approximations results indicates that the EP constraints have the effect to *decrease* drastically the shear modal effective EMCC.

Hard foam filling material case frequencies are listed in Table 2. They share comments on soft foam filling material results concerning *lower* host structure frequencies than adaptive ones and equality of f_{SC} and f_E frequencies. However, EP and NE frequencies are here very close for the first four modes.

From modal shapes visualizations, it can be noticed here that bending modes computed order of host structure (1, 2, **5**, 6, 8, 10) is different from that (1, 2, **4**, 6, 8, 10) of adaptive structures with SC and OC (EP, NE) electrodes and with patches having elastic properties (at constant electric fields E and displacements D), but this concerns only the 3rd x - z bending mode (in bold in Table 2)

Table 3 First six x-z bending modes frequencies of the adaptive sandwich beam with glue filled spaces

x-z bending modes	f_{hs} (Hz)	f_E (Hz)	f_{SC} (Hz)	f_{EP} (Hz)	f_{NE} (Hz)	f_D (Hz)
1	37.04	36.87	36.87	36.871	36.873	36.899
2	232	220.59	220.59	220.61	220.62	220.71
3	650.17	617.84	617.84	617.93	617.97	618.16
4	1276.5	1214.5	1214.5	1214.8	1215	1215.4
5	2116	1977.7	1977.7	1977.9	1978.5	1979.3
6	3171.3	3000.7	3000.7	3001.2	3002.7	3003.7

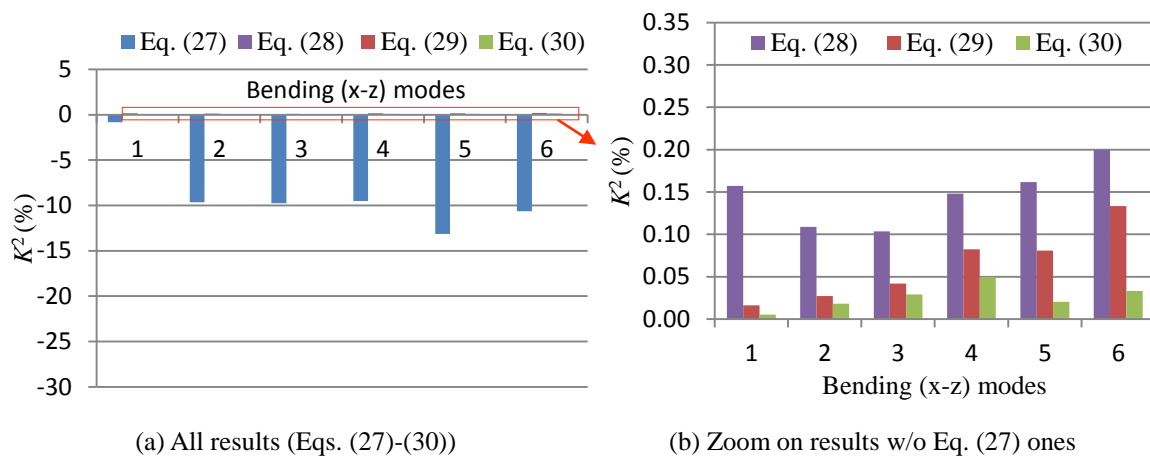


Fig. 9 Shear modal effective EMCC of the sandwich beam with glue as filling material

which has to be identified carefully from 3D FE computed modal shapes. The same local 3D foam effects as discussed above (see Fig. 5) are also observed here.

Post-treated modal effective EMCCs from Table 2 are shown in Fig. 8. The same comments, as for the soft foam filling material case, can be said for the present hard foam one.

Glue filling material's frequencies are listed in Table 3. They are *very different* from those of foam (soft or hard) filling materials. In particular, host structure frequencies are higher than those of adaptive structures. However, f_{SC} and f_E frequencies equality still holds. As for the hard foam case, EP and NE frequencies are very close to each other for the first four modes; however, EP constraints affect now mainly highest modes (last two ones) but almost not the lowest four ones.

Here, modal shapes visualizations indicate that the bending modes computed order of the host structure (1, 2, 4, 6, 8, 10) is *similar* to that of adaptive structures with SC and OC (EP, NE) electrodes and with the patches having elastic properties (at constant electric fields E) and displacements D). Besides, there are no local 3D foam effects in this case.

Modal effective EMCCs, post-treated from Table 3, are shown in Fig. 9. Here, host structure-based EMCC values are negative (Fig. 9(a)) due to the glue higher stiffness than foams ones. While EMCC variations with increasing modes are similar to those of previous foam cases, their values are *much lower*, since they do not exceed 0.2% for the most overestimating approximation.

4.3 Simplified analyses

This sub-section investigates the suitability of UDEF 2D PStrain and PStress models for simulating modal analysis of the benchmark (Fig. 3) with the three filling materials; the modal effective EMCC reference evaluation (Eq. (30)) is used as a coupled modes indicator. Here also, only beam-like bending (x - z) modes are considered for 2D simplified analyses assessments.

Soft foam filling material case frequencies are presented in Table 4 which shows that PStrain frequencies are higher than PStress ones for both SC and OC (with EP) electric conditions. Compared to 3D frequencies (considered hereafter as reference), as in Table 1 columns 4 (SC) and 5 (EP), PStress values are closer to references than PStrain ones. Also, 3D frequencies are bounded from below by PStress frequencies and from above by PStrain ones; these results confirm those obtained for the corresponding transverse –mode response setup (Benjeddou 2014).

Post-treated modal effective EMCCs from frequencies of Table 4 are shown in Fig. 10. The latter does not confirm totally results obtained for the extension setup (Benjeddou 2014) equivalent to the present shear one concerning the fact that 3D modal effective EMCC is, as frequencies, bounded from below by PStress EMCC and from above by PStrain one. Noticeably here are the *very low* EMCC values which do not exceed 0.05% for the optimum 4th mode. Besides, PStrain analysis provides nil EMCC for the first mode in contrary to 3D and PStress ones.

Table 5 lists *hard* foam case frequencies. Comments on the previous case are valid also here.

Post-treated modal effective EMCCs from Table 5 frequencies are shown in Fig. 11. Here, the first mode effective EMCC resulting from PStrain analysis is *not nil* and the other results change only for modes 5 and 6, where there is a performance exchange of PStrain and PStress analyses.

Table 4 2D first six x - z bending frequencies of the adaptive sandwich beam with *soft foam* filled spaces

2D modes	UDEF Plane Strain		UDEF Plane Stress	
	f_{SC} (Hz)	f_{EP} (Hz)	f_{SC} (Hz)	f_{EP} (Hz)
1	39.435	39.435	37.258	37.259
2	222.99	223.01	211.52	211.54
3	557.21	557.28	532.2	532.26
4	999	999.24	956.43	956.64
5	1459.3	1459.4	1395.7	1395.9
6	2115.7	2115.8	2019.5	2019.6

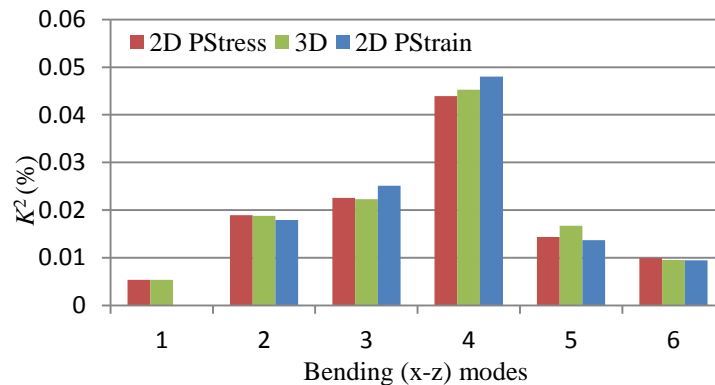


Fig. 10 2D vs. 3D modal effective EMCC of the sandwich beam with *soft foam* filling material

Table 5 2D first six x - z bending frequencies of the adaptive sandwich beam with *hard foam* filled spaces

2D modes	UDEF Plane Strain		UDEF Plane Stress	
	f_{SC} (Hz)	f_{EP} (Hz)	f_{SC} (Hz)	f_{EP} (Hz)
1	39.566	39.567	37.368	37.369
2	227.61	227.63	215.51	215.53
3	587.98	588.06	560.16	560.23
4	1070.2	1070.5	1023.4	1023.6
5	1563.8	1564	1498	1498.1
6	2247.1	2247.2	2150.7	2150.8

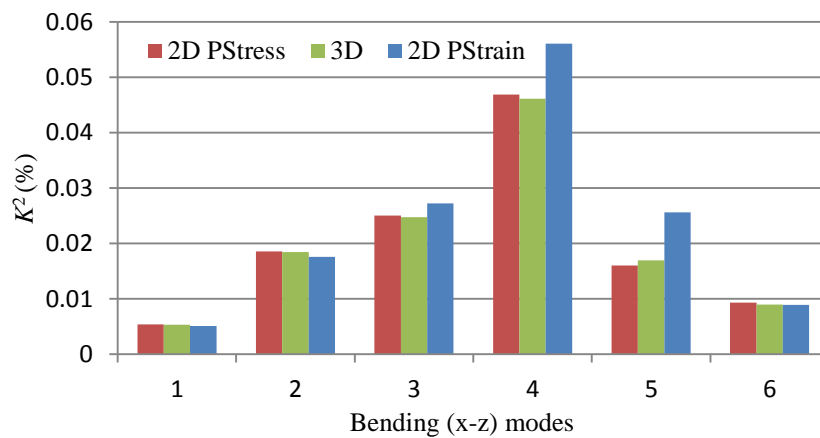


Fig. 11 2D vs. 3D modal effective EMCC of the sandwich beam with *hard foam* filling material

Table 6 2D first six x - z bending frequencies of the adaptive sandwich beam with *glue* filled spaces

2D modes	UDEF Plane Strain		UDEF Plane Stress	
	f_{SC} (Hz)	f_{EP} (Hz)	f_{SC} (Hz)	f_{EP} (Hz)
1	38.826	38.826	36.644	36.644
2	231.85	231.87	218.84	218.86
3	647.25	647.36	611.05	611.14
4	1264.6	1265	1194.2	1194.5
5	2043.6	2043.8	1930.549	1930.8
6	3073.7	3074.3	2904.8	2905.3

Table 6 shows *Glue* induced frequencies; it confirms comments on foams materials.

Modal effective EMCC results post-treated from Table 6 are illustrated in Fig. 12. Here, the first mode effective EMCC resulting from both PStrain and PStress analyses is nil and the other results also change for modes 5 and 6, where PStrain and PStress analyses exchange performance (closeness to 3D reference results).

It's worthy to notice that the shear modal effective EMCC reference evaluation performance depends on the filling material stiffness, as can be seen from Fig. 13, so that its increase enhances the modal effective EMCC. Fig. 13 shows also that, while soft and hard foams provide the same variations with increasing the bending (x - z) modes order, the glue behaves differently in the sense

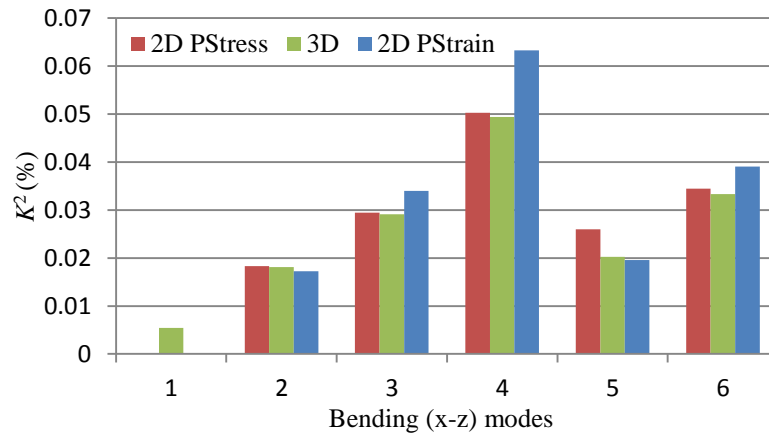


Fig. 12 2D vs. 3D modal effective EMCC of the sandwich beam with *glue* filling material

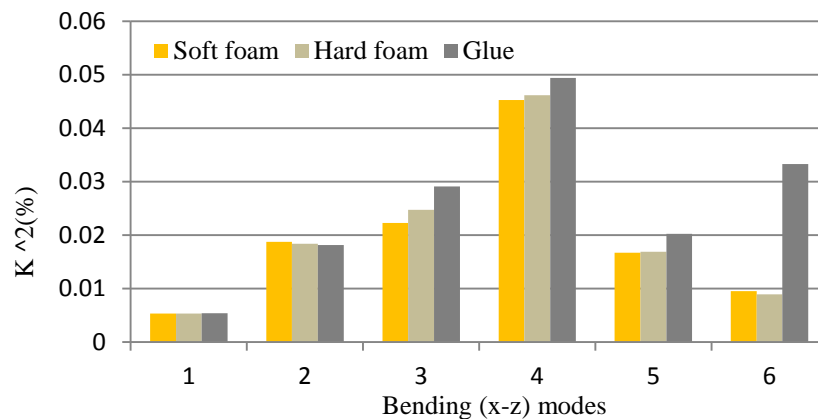


Fig. 13 Sandwich core filling material's influence on 3D shear modal effective EMCC reference evaluation

that the highest mode order (6) performance is not lower than the preceding mode one (5).

5. Conclusions, recommendations and perspectives

Shear modal effective EMCC approximate evaluations and UDEF PStrain and PStress simplified analyses have been *theoretically presented for the first time* and numerically assessed. For this purpose, 3D SOLID (hexahedral) ANSYS® piezoelectric and elastic FEs simulations have been presented for a typical sandwich cantilever beam benchmark. Soft foam, hard foam and glue were used as filling materials of the core spaces non-occupied by two shear piezoceramic patches under different electric conditions or for replacing them when considering a host structure.

It was found that the shear modal effective EMCC is highly sensitive to both *EP constraints* for OC electric conditions and to the *stiffness* of the material filling the spaces non-occupied by the transducers. Besides 2D PStrain and PStress simplified analyses comparison to 3D simulations confirmed that 3D SC and OC frequencies are bounded from below by PStress values and from

above by PStrain ones. However, for the modal effective EMCC, this was only true for few modes; hence, equivalent transverse-mode setup results (Benjeddou 2014) are only *partially confirmed*. Another important result is that the shear modal effective EMCC reference values were found *too low*, in particular for its potential use in shunted damping and energy harvesting applications.

As recommendations to researchers and engineers, it is mandatory to *enforce the physical EP constraints* in any OC analysis; also, the popular *host-structure based approximate evaluation has to be avoided* for the shear modal effective EMCC. Besides, when coupled piezoelectric FE analysis is not available, elastic one can be used together with the transducers' elastic properties (at constant electric fields or displacements). However, it should be kept in mind that this approximation cannot see electromechanically uncoupled modes and the resulting modal effective EMCC are overestimated; this is also true for piezoelectric FE analysis without enforcing EP constraints which are equivalent to NE conditions. Hence, these *approximate evaluations are helpful only for preliminary or pre-design analysis*. As a simplified analysis, *prefer PStress* one.

Immediate extension and application of the present work could be directed, respectively, to EMCC experimental measurements for shear-mode benchmarks (Berik *et al.* 2011) and to *structural vibration shear energy harvesting theoretical and practical investigations*.

Acknowledgments

Support of the Austrian Comet K2 Linz Center of Mechatronics (LCM) is gratefully acknowledged. The author is also thankful to his students (S. Simon and A. Berson) for running ANSYS® FE simulations under his supervision.

References

- Abramovitch, H. (2003), "Piezoelectric actuation for smart sandwich structures-closed form solutions", *J. Sandwich Struct. Mater.*, **5**(4), 377-396.
- Aladwani, A., Aldraihem, O. and Baz, A. (2013), "Single degree of freedom shear-mode piezoelectric energy harvester", *ASME J. Vib. Acoust.*, **135**(5), 051011.
- Baillargeon, B.P. and Vel, S.S. (2005a), "Exact solution for the vibration and active damping of composite plates with piezoelectric shear actuators", *J. Sound Vib.*, **282**(3-5), 781-804.
- Baillargeon, B.P. and Vel, S.S. (2005b), "Active vibration suppression of sandwich beams using piezoelectric shear actuators: experiments and numerical simulations", *J. Intel. Mater. Syst. Struct.*, **16**(6), 517-530.
- Benjeddou, A. (2000), "Advances in piezoelectric finite element modeling of adaptive structural elements: a survey", *Comput. Struct.*, **76**(1-3), 347-363.
- Benjeddou, A. (2006), "First use of the shear piezoceramics and effective electromechanical coupling coefficient for damage detection and characterization", *Proceedings of the III European Workshop on Structural Health Monitoring*, Granada, Spain, July.
- Benjeddou, A. (2007), "Shear-mode piezoceramic advanced materials and structures: a state of the art", *Mech. Adv. Mater. Struct.*, **14**(4), 263-275.
- Benjeddou, A. (2009), "New insights in piezoelectric free-vibrations using simplified modeling and analyses", *Smart Struct. Syst.*, **5**(6), 591-612.
- Benjeddou, A. (2010), "Approximate evaluations of the modal effective electromechanical coupling coefficient", *Proceedings of the IUTAM Symposium on Multi-Functional Material Structures and Systems*, IUTAM Book series 19, Springer, Dordrecht.

- Benjeddou, A. (2014), "Modal effective electromechanical coupling approximate evaluations and simplified analyses: numerical and experimental assessments", *Acta Mech.*, **225**(10), 2721-2742.
- Benjeddou, A. and Belouettar, S. (2006), *On the evaluation and application of piezoelectric adaptive structures modal properties*, Innovation in Computational Structures Technology, Saxe-Coburg Publications, Stirlingshire, UK.
- Benjeddou, A. and Ranger, J.A. (2006), "Use of shunted shear-mode piezoceramics for structural vibration passive damping", *Comput. Struct.*, **84**(22-23), 1415-1425.
- Berik, P., Benjeddou, A., Brandl, A. and Krommer, M. (2011), "Experimental evaluation of the electromechanical coupling of smart structures with d_{15} shear-mode piezoceramic cores", *Proceedings of the 22nd International Conference on Adaptive Structures and Technologies*, Corfu, Greece, October.
- Boudaoud, H., Benjeddou, A., Daya, E.M. and Belouettar, S. (2007), "Analytical evaluation of the effective EMCC of sandwich beams with a shear-mode piezoceramic core", *Proceedings of the 2nd International Congress on Design and Modelling of Mechanical Systems*, Monastir, Tunisia, March.
- Cao, W., Zhu, S. and Jiang, B. (1998), "Analysis of shear modes piezoelectric vibrator", *J. Appl. Phys.*, **83**(8), 4415-4420.
- De Godoy, C.T. and Trindade, M.A. (2011), "Modeling and analysis of laminate composite plates with embedded active passive piezoelectric networks", *J. Sound Vib.*, **330**, 194-216.
- Deü, J.F. and Benjeddou, A. (2005), "Free-vibration analysis of laminated plates with embedded shear-mode piezoceramic layers", *Int. J. Solid. Struct.*, **42**(7), 2059-2088.
- Dos Santos, H.F.L. and Trindade, M.A. (2011), "Structural vibration control using extension and shear active-passive piezoelectric networks including sensitivity to electrical uncertainties", *J. Braz. Soc. Mech. Sci. Eng.*, **33**(3), 287-301.
- Ederly-Azulay, L. and Abramovitch H. (2006), "Active damping of piezo-composite beams", *Comput. Struct.*, **74**, 458-466.
- IEEE Inc. (1988), *IEEE Standard on Piezoelectricity*, ANS/IEEE Std 176-1987.
- Kim, J.S., Wang, K.W. and Smith, E.C. (2005), "High authority piezoelectric actuation system synthesis through mechanical response and electrical tailoring", *J. Intel. Mater. Syst. Struct.*, **16**(1), 21-31.
- Majidi, C., Haataja, M. and Srolowitz, D.J. (2010), "Analysis and design principles for shear-mode piezoelectric energy harvesting with ZnO nanoribbons", *Smart Mater. Struct.*, **19**, 055027.
- Manjunath, T.C. and Bandyopadhyay, B. (2006), "Design of multivariable POF controller for smart composite beam using embedded shear sensors and actuators", *Int. J. Simul. Syst. Sci. Tech.*, **7**(9), 49-69.
- Ren, B., Or, S.W., Zhang, Y., Zhang, Q., Li, X., Jiao, J., Wang, W., Liu, D., Zhao, X. and Luo, H. (2010), "Piezoelectric energy harvesting using shear mode $0.71\text{Pb}(\text{Mg}_{1/3}\text{Nb}_{2/3})\text{O}_3$ - 0.29PbTiO_3 single crystal cantilever", *Appl. Phys. Lett.*, **96**, 083502.
- Trindade, M.A. and Benjeddou, A. (2009), "Effective electromechanical coupling coefficients of piezoelectric adaptive structures: critical evaluation and optimization", *Mech. Adv. Mater. Struct.*, **16**(3), 210-223.
- Trindade, A.M. and Maio, C.E.B. (2008), "Multimodal passive vibration control of sandwich beams with shunted shear piezoelectric materials", *Smart Mater. Struct.*, **17**(5), 055015..
- Wang, D.A. and Liu, N.Z. (2011), "A shear mode piezoelectric energy harvester based on pressurized water flow", *Sens. Act. A: Phys.*, **167**, 449-458.
- Zhao, J.H., Zheng, X.J., Zhou, L., Zhang, Y., Sun, J., Dong, W., Deng, S.F. and Peng, S.T. (2012), "Investigation of a d_{15} mode PZT-51 piezoelectric energy harvester with a series connection structures", *Smart Mater. Struct.*, **21**, 105006.
- Zhou, L., Sun, J., Zheng, X.J., Deng, S.F., Zhao, J.H., Peng, S.T., Zhang, Y., Wang, X.Y. and Cheng, H.B. (2012), "A model for the energy harvesting performance of shear mode piezoelectric cantilever", *Sens. Act. A: Phys.*, **179**, 185-192.

Abbreviations

1D: One-dimensional

2D: Two-dimensional

3D: Three-dimensional

BC: Boundary condition

D: Superscript used for piezoelectric material elastic matrix at constant electric displacements

DOF: Degree of freedom

E: Superscript used for piezoelectric material elastic matrix at constant electric fields

EMCC: Electromechanical coupling coefficient (structural)

EMCF: Electromechanical coupling factor (material)

EP: equipotential

ESL: Equivalent single layer

FE: Finite element

hs: host structure

MSE: Modal strain energy

NE: non-electroded

OC: Open circuit

PStrain: Plane strain

PStress: Plane stress

SC: Short circuit

SDOF: Single degree of freedom

UDEF: Unidirectional electric field

VF: Variational formulation

w: with

w/o: without

Appendix

The beam and filling materials are elastic and isotropic; their assumed properties are summarized in Table 7.

Table 7 Properties of the beam faces and core filling materials

Material Constants	Beam faces	Sandwich core filling material		
		Soft foam	Hard foam	Glue
Young's modulus (MPa)	73,000	35.3	62	10,000
Poisson's ratio	0.33	0.38	0.35	0.3
Mass density (Kg/m ³)	2,790	32	80	1,100

SC properties of PZT-5A with polarization along x -axis are obtained from the rotation of those which polarization is along the thickness (Benjeddou 2009)

$$[C_{p//x}^E] = \begin{bmatrix} 86.856 & 50.778 & 50.778 & 0 & 0 & 0 \\ 50.778 & 99.201 & 54.016 & 0 & 0 & 0 \\ 50.778 & 54.016 & 99.201 & 0 & 0 & 0 \\ 0 & 0 & 0 & 22.593 & 0 & 0 \\ 0 & 0 & 0 & 0 & 21.1 & 0 \\ 0 & 0 & 0 & 0 & 0 & 21.1 \end{bmatrix} \text{ (GPa)} \quad (51a)$$

$$[e_{p//x}] = \begin{bmatrix} 15.118 & -7.209 & -7.209 & 0 & 0 & 0 \\ 0 & 0 & 0 & 0 & 0 & 12.322 \\ 0 & 0 & 0 & 0 & 12.322 & 0 \end{bmatrix} \text{ (C/m}^2\text{)} \quad (51b)$$

$$[\epsilon_{p//x}^S] = \begin{bmatrix} 6.880 & 0 & 0 \\ 0 & 8.104 & 0 \\ 0 & 0 & 8.104 \end{bmatrix} \text{ (nF/m)} \quad (51c)$$

The PZT-5A mass density is $\rho=7700 \text{ Kg/m}^3$ and its shear EMCF is $k_{15}=0.69$ (Benjeddou 2009).

From Eqs. (51a)-(51c), the PZT-5A full OC elastic matrix is also obtained by rotation of that corresponding to the thickness poled case (Benjeddou 2009) as (only non-nil terms are given)

$$[C_{p//x}^D] = \begin{bmatrix} 120.07 & 34.94 & 34.94 & \vdots & \vdots & \vdots \\ 34.94 & 106.75 & 61.57 & \vdots & \vdots & \vdots \\ 34.94 & 61.57 & 106.75 & \vdots & \vdots & \vdots \\ \vdots & \vdots & \vdots & 22.59 & \vdots & \vdots \\ \vdots & \vdots & \vdots & \vdots & 39.83 & \vdots \\ \vdots & \vdots & \vdots & \vdots & \vdots & 39.83 \end{bmatrix} \text{ (GPa)} \quad (52)$$